Enhanced Radar Backscattering due to Oriented Ice Particles at 95 GHz during StormVEx

ROGER MARCHAND

Department of Atmospheric Sciences, University of Washington, Seattle, Washington

GERALD G. MACE

Department of Atmospheric Sciences, University of Utah, Salt Lake City, Utah

A. GANNET HALLAR AND IAN B. MCCUBBIN

Division of Atmospheric Sciences, Desert Research Institute, Reno, Nevada, and Storm Peak Laboratory, Steamboat Springs, Colorado

SERGEY Y. MATROSOV AND MATTHEW D. SHUPE

Cooperative Institute for Research in Environmental Sciences, University of Colorado Boulder, and NOAA/Earth System Research Laboratory, Boulder, Colorado

(Manuscript received 20 December 2012, in final form 13 April 2013)

ABSTRACT

Nonspherical atmospheric ice particles can enhance radar backscattering and attenuation above that expected from spheres of the same mass. An analysis of scanning 95-GHz radar data collected during the Storm Peak Laboratory Cloud Property Validation Experiment (StormVEx) shows that at a least a small amount of enhanced backscattering was present in most radar scans, with a median enhancement of 2.4 dB at zenith. This enhancement will cause an error (bias) in ice water content (IWC) retrievals that neglect particle orientation, with a value of 2.4 dB being roughly equivalent to a relative error in IWC of 43%. Of the radar scans examined, 25% had a zenith-enhanced backscattering exceeding 3.5 dB (equivalent to a relative error in IWC in excess of 67%) and 10% of the scans had a zenith-enhanced backscattering exceeding 6.4 dB (equivalent to a relative error in IWC in excess of 150%). Cloud particle images indicate that large enhancement typically occurred when planar crystals (e.g., plates and dendrites) were present, with the largest enhancement occurring when large planar crystals were falling out of a supercooled liquid-water layer. More modest enhancement was sometimes due to planar crystals, but it was also sometimes likely a result of horizontally oriented nonspherical irregularly shaped particles. The analysis also shows there is a strong correlation (about −0.79) between the change in slant 45° depolarization ratio with radar scan elevation angle and the magnitude of the zenith-enhanced backscattering, suggesting that measurements of the slant depolarization ratio can be used to improve radar-based cloud microphysical property retrievals.

1. Introduction

It has long been known that nonspherical atmospheric ice particles can increase or enhance radar backscattering and attenuation above that expected from spheres of the same mass, even when the particles are small compared with the radar wavelength (e.g., Atlas et al. 1953). This is particularly true when nonspherical ice particles are oriented such that their largest dimension is perpendicular to the radar beam. Because of aerodynamic effects, both planar ice crystals (such as plates and dendrites) and columnar crystals tend to fall with their larger dimension near horizontal. As a result, reflectivity measurements from near-zenith-pointing ground-based radars and near-nadir-pointing spaceborne radars are potentially prone to being affected by ice crystal orientation. This includes the National Aeronautics

Corresponding author address: Roger Marchand, Department of Atmospheric Sciences, University of Washington, 408 ATG Building, Seattle, WA 98195-1640.
E-mail: rojmarch@u.washington.edu

DOI: 10.1175/JTECH-D-13-00005.1

and Space Administration (NASA) *CloudSat* radar (Stephens et al. 2008) and the ground-based radars that have been deployed for many years by the U.S. Department of Energy (DOE) Atmospheric Radiation Measurement Program (ARM; e.g., Clothiaux et al. 2000), among others. Enhanced backscattering for zenith and near-nadir-pointing radars (relative to what would be expected for spheres of the same mass or relative to off-nadir viewing) tends to increase with the size of the cloud particles and with the radar frequency, but non-Rayleigh scattering effects are important at 95 GHz and higher frequencies, as ice particles often reach sizes that are not small compared to the radar wavelength at these frequencies. Electromagnetic modeling of scattering at 95 GHz with the discrete dipole approximation by Okamoto (2002) indicates that for small particles (effective radius $< 100\,\mu$m), the effect of plate and column orientation on radar (copolar) reflectivity is less than 2 dB, but for larger particles differences can be as large as 8 dB.

In spite of this potentially large enhancement in radar reflectivity, few cloud microphysical retrievals using 95-GHz radar reflectivity data have taken ice particle orientation into consideration, and instead generally treat ice particles as spheres or randomly oriented ice crystals. Exceptions include the experimental retrieval of ice water content by Matrosov and Heymsfield (2008) and the variational radar–lidar ice cloud (VarCloud) retrieval created by Delanoë and Hogan (2010) and extended by Stein et al. (2011). These retrievals assume horizontally aligned oblate spheroids with a fixed axial ratio of 0.6 for ice cloud particles. These authors found that using a spheroidal assumption in the same retrieval produces a retrieved ice water content that is reduced by on average 50% in clouds with a reflectivity factor larger than 0 dBZ.

There are at least two reasons why the effect of oriented ice crystals is not commonly incorporated into radar-based retrievals. One is that while planar crystals are at times found in aircraft in situ observations, many clouds appear to contain few such crystals, especially midlatitude clouds with temperatures below −20°C (Korolev et al. 2000; Heymsfield 2003). Korolev et al. analyzed in situ observations of particles with maximum dimensions greater than 125 μm in size, from several aircraft flights. These authors found that while the maximum frequency of occurrence of dendrites is much larger at temperatures above −20°C than below −20°C, even at warmer temperatures the majority of cases showed no dendrites at all. Rather, they found the dominant ice particle habit to be irregular particles and that dendritic ice particles tend to occur in isolated cells embedded in zones of irregularly shaped ice particles. In such cells the fraction of dendrites was often large and reached 100%. Assuming oriented particles are present in a radar-based retrieval will result in equally large errors (underestimates) of ice water content when they are not present.

On the other hand, the frequent presence of oriented ice crystals has been inferred from ground-based (scanning) lidar depolarization measurements (e.g., Sassen and Benson 2001; Westbrook et al. 2010), in some aircraft measurements in mixed-phase altocumulus (e.g., Carey et al. 2008; Hogan et al. 2003), in the analysis of cloud-top visible wavelength polarized reflectances (e.g., Chepfer et al. 1999; Noel and Chepfer 2004), and in the analysis of NASA *Cloud–Aerosol Lidar and Infrared Pathfinder Satellite Observations* (*CALIPSO*) lidar depolarization observations of both ice and mixed-phase clouds (Noel and Chepfer 2010; Sassen et al. 2012; Zhou et al. 2012). The effect of specular reflection from oriented crystals was sufficiently problematic for *CALIPSO* ice cloud microphysical retrievals that the lidar pointing was eventually changed from the original 0.3° off-nadir pointing to 3° off-nadir pointing, in order to reduce greatly its occurrence and strength. The fraction of particles responsible for causing this specular reflection is not very large. Zhou et al. (2012) estimate the fraction of such particles to range from 0% to 6% for mixed-phase clouds and from 0% to 3% for ice clouds with temperatures greater than −35°C. Though few in number, if these crystals are large enough, then they will nonetheless significantly increase or perhaps even dominate the observed radar reflectivity.

A second reason the effect of oriented ice crystals is not often incorporated into radar-based retrievals is that few available remote sensing observations provide a signal that is uniquely or predominantly a response to particle orientation, and extracting information on orientation generally requires simultaneously determining the particle size and the particle shape to some degree. The aforementioned lidar depolarization measurements, for example, do contain information on particle orientation. However, combining radar and lidar data requires assumptions on how the shape and ratio of oriented to nonoriented particles change with particle size, because scattering at radar wavelengths is generally much stronger from the larger particles in the particle size distribution, while visible light (lidar) scatters efficiently from small ice particles and is typically dominated by the much more numerous small particles. In spite of these difficulties, Okamoto et al. (2010) have developed a *CloudSat–CALIPSO* radar–lidar retrieval that uses the measured radar reflectivity, lidar backscatter, and lidar depolarization ratio in combination with scattering models for horizontally oriented plates (with an assumed aspect ratio of 3) and various sets of

randomly oriented ice or ice spheres. These authors found that this algorithm retrieves significantly larger effective radius and smaller ice water content (at times an order of magnitude different) than the same algorithm when polarization data and horizontal plates are not used. The largest errors typically occurred in the temperature range between −20° and −10°C, where the retrieved effective radius was greater than 200 μm. Of course, a combined lidar–radar approach is limited to those cloudy regions where the lidar has not been heavily attenuated, and it generally requires accounting for multiple scattering where the lidar does penetrate.

While not measured by *CloudSat*, 95-GHz radar depolarization measurements have also seen some investigation of their potential to retrieve (or at least provide constraints on) cloud ice particle type and orientation (Aydin and Tang 1997; Matrosov et al. 2001; Reinking et al. 2002; Aydin and Singh 2004), and this includes combining radar observations of different depolarization types (Matrosov et al. 2005). Nonetheless, we are not aware of any operational algorithms (or even large observational datasets) where retrieved ice particle type and orientation are obtained from millimeter-wavelength radar reflectivity and depolarization measurements.

In this article, in situ cloud microphysical observations and scanning 95-GHz (W band) polarimetric radar data, gathered during the Storm Peak Laboratory Cloud Property Validation Experiment (StormVEx), are used to characterize the frequency and strength of enhanced backscattering due to oriented ice crystals, as well as to investigate the relationship between enhanced backscattering and slant linear 45° depolarization ratio measurements. The main reason a slant linear configuration was used during StormVEx is because slant linear is expected to be less susceptible to small flutter in the horizontal orientation of particles than the more traditional horizontal–vertical linear depolarization ratio (LDR; Reinking et al. 2002). StormVEx was conducted between November 2010 and April 2011 (Mace et al. 2010). Storm Peak Laboratory (SPL) is a mountain-top station located near Steamboat Springs, Colorado. With an altitude of 3220 m, this station is frequently in cloud during the winter months (Borys and Wetzel 1997). One of the primary achievements of this experiment was the acquisition of a large collaborative dataset of remote sensing data and in situ measurements in liquid, ice, and mixed-phase clouds. During StormVEx, the U.S. DOE ARM deployed a suite of remote sensing equipment near SPL, and the extensive array of aerosol measurement equipment normally operated at SPL (Hallar et al. 2011a,b) was expanded to include a variety of cloud particle probes.

Previously, Matrosov et al. (2012) (the same authors as the present study) published a case study analysis of the radar slant linear depolarization ratio measured during StormVEx. This article examines individual cases with rounded graupel, pristine dendrites, rimed dendrites, and a mixture of graupel, dendrites, and columns. The study shows that changes in the measured slant depolarization ratio between zenith and off-zenith angles are indicative either of planar or columnar ice crystals. The present study extends this earlier work, presenting a statistical analysis from thousands of radar scans, as well as focusing on the effects of oriented crystals on the (copolar) reflectivity. In section 2, the technique used to identify and estimate the magnitude of enhanced backscattering from the scanning radar data is described, and in section 3 these data are analyzed in the context of the in situ cloud data gathered at SPL. Section 4 provides additional discussion.

2. Scanning radar data

During StormVEx, the scanning W-band ARM cloud radar (SWACR) was positioned approximately 2.4 km southwest and just over 400 m below SPL. The radar rotated through a fixed sequence of modes, which included making six range–height indicator (RHI) horizon-to-horizon scans at six different azimuth angles, about once each half-hour. Figures 1–3 each show examples of the observed radar (copolar) reflectivity (top-left panels) and depolarization ratio (top-right panels). The depolarization ratio (DR) in decibels (dB) is defined as

$$\mathrm{DR} = \mathrm{dB}(Z_{\text{cross-polar}}) - \mathrm{dB}(Z_{\text{copolar}}), \qquad (1)$$

where $\mathrm{dB}(Z) = 10\log_{10}(Z)$, $Z_{\text{cross-polar}}$ is the cross-polar reflectivity factor, and $Z_{\text{co-polar}}$ is the copolar reflectivity factor (both having units of $\mathrm{mm}^6\,\mathrm{m}^{-3}$). During StormVEx, the radar was configured to use slant linear 45° depolarization as discussed by Matrosov et al. (2012). Because attenuation by gases and small liquid drops is the same at both polarizations, DR is unaffected by these sources of attenuation as long as there is sufficient signal-to-noise ratio in both measurements. The radar data shown in these panels have been limited to those regions where the signal exceeds the estimated radar noise by 3 dB (approximately −35 dBZe at 1 km). The copolar reflectivity in Fig. 1 shows a narrow column of large reflectivity (values near 10 dBZe) directly above the radar, with significantly smaller values on either side. The large reflectivity values directly above the radar are not because of some unusual cloud that just happened to be centered over the radar at the time of this scan; this

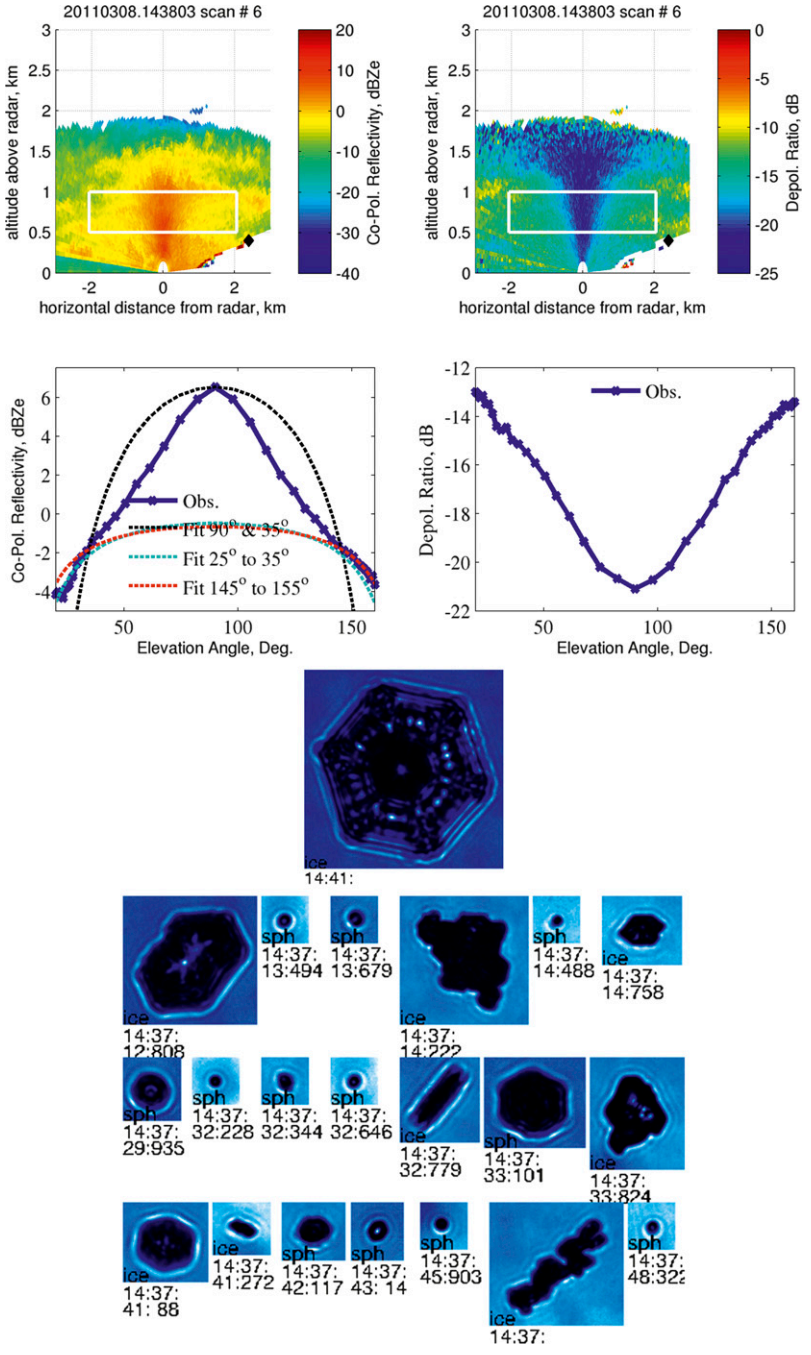

FIG. 1. Example of radar data showing large enhanced backscattering effect: (top left) copolar 95-GHz scanning radar reflectivity; (top right) slant 45° DR; (middle left) radar copolar reflectivity vs scan (elevation) angle for the region 0.5–1 km above the radar (white box shown in top left); and (middle right) DR vs elevation angle for the same region. Black diamond shows location of SPL. Elevation angles away from zenith (elevation = 90°) are farther from the radar and so are expected to show a reduction in reflectivity because of increased path attenuation. Dashed lines show the fit of a simple model where radar reflectivity is only due to randomly oriented particles and path attenuation. The fit is determined using the observed reflectivity at elevation angles of zenith and 35° (black line), 25°–35° (light blue line), and 145°–155° (red line). The poor fit of the black line to the observations, as well as between black and colored lines, demonstrates that the change in reflectivity with the scan angle is not because of path attenuation and that scattering from oriented ice particles is important; see text. (bottom) Images of sample cloud particles taken by the CPI. The large particle at the top is 300 μm wide, and all the images are to scale.

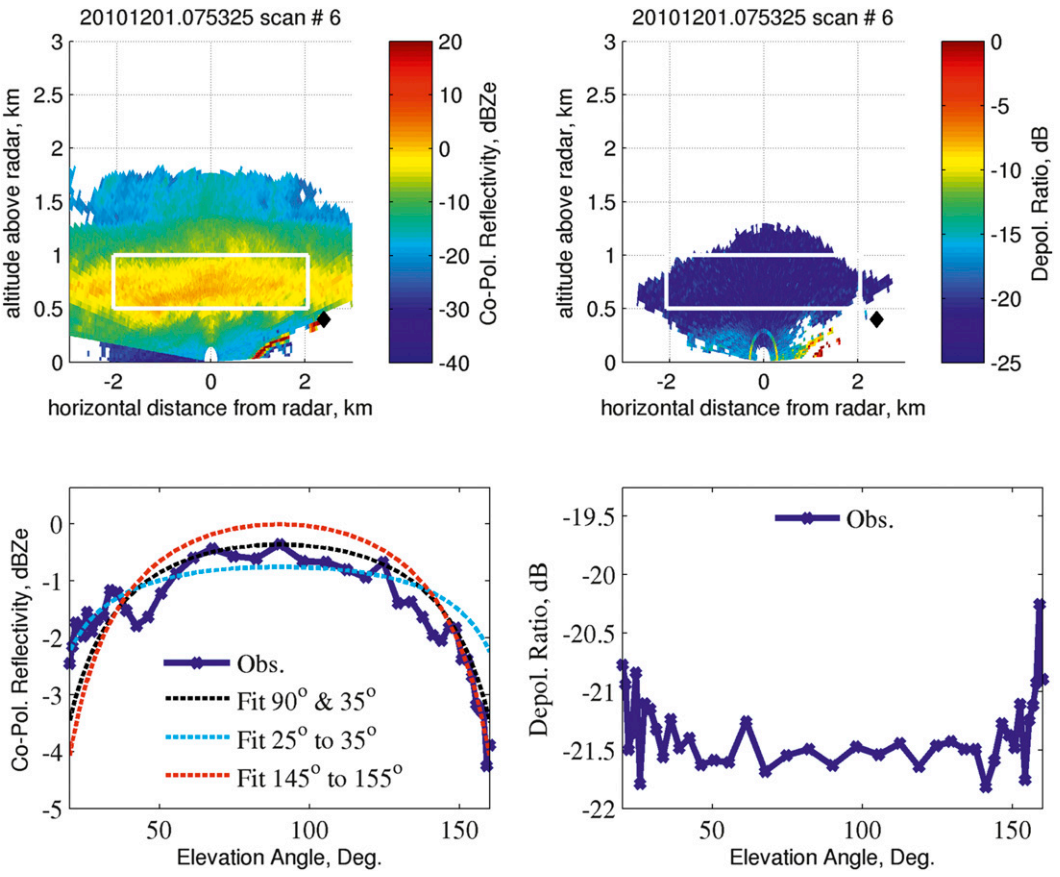

FIG. 2. As in Fig. 1, but for a case with no reflectivity enhancement at nadir. Microphysical observations at SPL show this cloud consisted of water droplets with a few heavily rimed ice particles. Images of sample cloud particles not shown.

same feature is observed in all six radar scans undertaken at this time (each about 1 min apart), and similar features are seen in a significant fraction of the RHI scans acquired during the experiment. Rather, we contend that the large values of reflectivity in Fig. 1 and in most of the other instances of this phenomenon are because of enhanced backscattering by oriented ice crystals. The radar depolarization ratio in the top-right panel of Fig. 1 shows a cone with low depolarization values directly above the radar and increasing values of depolarization on both sides for altitudes between the surface and 1.5 km. As discussed by Matrosov et al. (2012), this pattern in the slant depolarization ratio is expected for horizontally oriented planar ice crystals, and indeed the cloud particle imager (CPI) at SPL showed that this cloud contained a variety of particle types including planar ice crystals. The CPI is a single-particle imaging probe that captures 2D images of particles using a charge-coupled device (CCD) camera with an image resolution of about 2.3 μm, and is capable of imaging particles of up to about 2 mm (Lawson et al. 2001). A sample of CPI images is shown at the bottom of Fig. 1. The largest plate shown here is about 300 μm wide.

Near the top of the cloud in Fig. 1 (above about 1.5 km), depolarization values remain low, showing little if any change with the scan angle. Low depolarization values with no scan angle dependence are indicative of quasi-spherical ice particles or small water droplets (Matrosov et al. 2012). Figure 2, for example, shows results for a cloud primarily composed of liquid water but also containing some heavily rimed irregularly shaped ice particles. Figure 1 shows little if any enhancement in near-zenith radar reflectivity above 1.5 km, which is indicative of there being few (if any) oriented ice crystals and consistent with the low depolarization ratio at all elevation angles in this region.

While the presence of enhanced backscattering is obvious in Fig. 1, more often the effect is significantly more subtle. Figure 3, for example, shows a more typical case. In this case, CPI observations show the cloud was mixed phase, almost entirely composed of water droplets, and relatively small planar ice crystals (with maximum

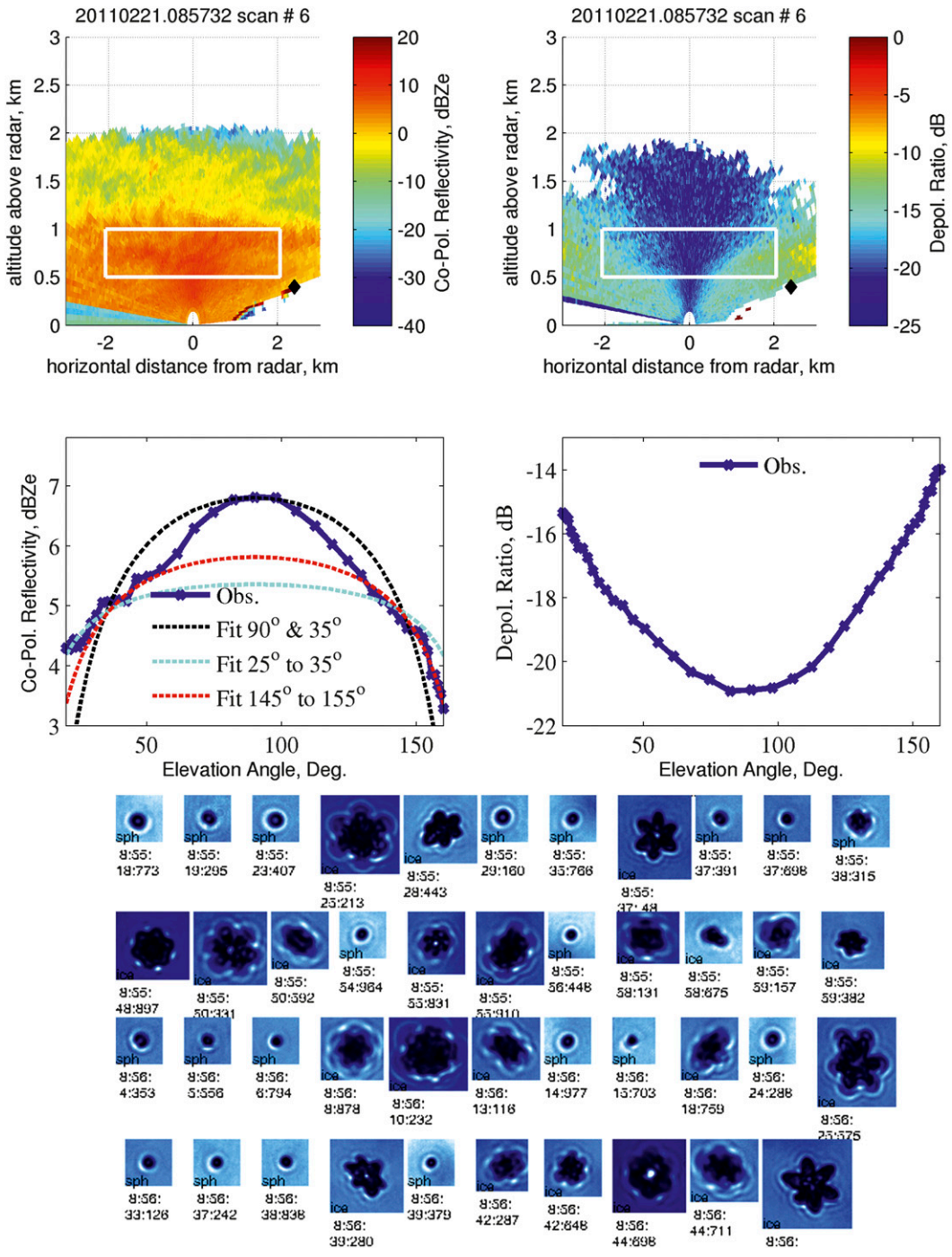

FIG. 3. As in Fig. 1, but for a case where reflectivity enhancement in copolar reflectivity is small (though still discernible). The presence of oriented ice crystals remains easily discernible from the change in slant 45° depolarization ratio with elevation angle. Microphysical observations at SPL show this cloud consisted of a mix of water droplets and small (max dimension < about 200 μm) planar crystals.

dimensions generally less than 200 μm). The small magnitude of the enhanced backscattering is likely because of the small size of the planar crystals in this case. However, it is also possible there are some large particles in this cloud that are partly responsible for the enhanced backscattering, and which were not sampled by the CPI because they were relatively few in number. Sampling limitations of the CPI are discussed later in this section.

While the effect of enhanced backscattering is much less obvious in the copolar radar reflectivity, the signature of planar ice crystals remains strong in the depolarization ratio.

The bottom-left panels of Figs. 1–3 show the mean radar reflectivity in the altitude range between 0.5 and 1 km above the radar, as a function of the radar scan elevation angle for elevation angles between 20° and 160°. This region is denoted by the white box in the top panels. All three figures show a peak in reflectivity near zenith (elevation angle of 90°), with the reflectivity decreasing away from zenith. Because the altitude is fixed, the farther the angle from zenith, the longer the pathlength through the atmosphere becomes; and one expects a larger path attenuation. Assuming horizontally homogenous conditions, one can write

$$\mathrm{dB}[Z_{\mathrm{obs}}(\theta_{\mathrm{el}})] = \mathrm{dB}(Z_{\mathrm{cloud}}) - \mathrm{Atten} \times \mathrm{dist}(\theta_{\mathrm{el}}), \qquad (2)$$

where Z_{obs} is the observed copolar reflectivity (units of $\mathrm{mm}^6\,\mathrm{m}^{-3}$) and depends on the elevation angle θ_{el}; Z_{cloud} is the copolar reflectivity of the cloud particles (which in the absence of oriented particles will be independent of the elevation angle and also in $\mathrm{mm}^6\,\mathrm{m}^{-3}$); Atten is the path attenuation at zenith (which includes attenuation resulting from both gasses and cloud particles in $\mathrm{dB\,km}^{-1}$); and dist is the distance from the radar to the reflectivity observation point (km). Thus, for homogenous conditions and in the absence of oriented particles, one can determine Z_{cloud} and Atten from Z_{obs} at any two elevation angles. The black dashed lines in Fig. 1 show how this equation compares to the observations when Z_{cloud} and Atten are determined using elevation angles of 35° and 90°. The black line fits the observed reflectivities rather poorly in Fig. 1. There is no choice for Atten that fits the observations for all elevation angles. This demonstrates that Z_{cloud} varies with the elevation angle, which we attribute to nonspherical horizontally oriented ice particles.

Rewriting Eq. (2) to allow the cloud reflectivity to vary with elevation angle—that is, an enhanced backscattering (EB) term—we obtain

$$\mathrm{dB}[Z_{\mathrm{obs}}(\theta_{\mathrm{el}})] = \mathrm{dB}(Z_{\mathrm{const}}) + \mathrm{dB}[Z_{\mathrm{EB}}(\theta_{\mathrm{el}})] - \mathrm{Atten} \times \mathrm{dist}(\theta_{\mathrm{el}}), \qquad (3)$$

where Z_{const} is the component of the cloud reflectivity that does not change with the elevation angle and Z_{EB} accounts for the change in reflectivity due to oriented particles. The total cloud reflectivity (constant + enhanced backscattering) is given by $\mathrm{dB}[Z_{\mathrm{cloud}}(\theta_{\mathrm{el}})] = \mathrm{dB}(Z_{\mathrm{const}}) + \mathrm{dB}[Z_{\mathrm{EB}}(\theta_{\mathrm{el}})]$, or equivalently $Z_{\mathrm{cloud}}(\theta_{\mathrm{el}}) = Z_{\mathrm{const}} \times Z_{\mathrm{EB}}(\theta_{\mathrm{el}})$. It is somewhat unintuitive but note that Z_{EB} has no units. It is a multiplicative factor [or equivalently, an additive factor when using a logarithmic representation as is done in Eq. (3)].

Having examined hundreds of radar RHI scans collected during StormVEx, we have found that (when horizontally homogenous conditions occur) observations at low elevation angles are consistently well modeled by Eq. (2), such as in Fig. 2, and are frequently accompanied by a change in the slope of the observed reflectivity curve with elevation angle (an inflection point), typically between about 35° and 50°, such as in Fig. 3. In our analysis, we assume that the change in the observed reflectivity at low elevation angles (specifically elevation angles lower than 35° or greater than 145°) is predominately due to attenuation and Z_{EB} is small compared with Z_{const} [i.e., $\mathrm{dB}Z_{\mathrm{EB}}(\theta_{\mathrm{el}} < 35°$ or $\theta_{\mathrm{el}} > 145°) \ll \mathrm{dB}Z_{\mathrm{const}}$] and can be neglected. We can thus fit Eq. (2) to the observations at these low angles to determine Z_{const} and Atten. This assumption may not always be valid, and we will discuss the implications of this assumption further in the following section. Using the observed reflectivity at zenith along with Z_{const} and Atten (determined from reflectivity measurements at low elevation angles), the zenith-enhanced backscattering $\mathrm{dB}[Z_{\mathrm{EB}}(90°)]$ is then readily obtained from Eq. (3).

The dashed red and cyan lines in Figs. 1–3 show the results of fitting Eq. (2) to the observations using data in the intervals 25°–35° and 145°–155°. The two solutions are not identical because of spatial heterogeneity in the observed cloud reflectivity. In our analysis, we use the difference in these two solutions to identify homogeneous cases, and include only cases where the estimated zenith-enhanced backscattering differs by no more than 1.5 dB, the estimated path attenuation differs by no more than 1 dB, and the estimated path attenuation is positive. This last condition removes cases where there is a gap (or thin cloud region) directly above the radar that is surrounded by equally reflective cloud on both sides—a rare occurrence. The retrieved value is taken as the average of the two estimates. Applying this approach, the example in Fig. 1 yields an estimate for the zenith-enhanced backscattering of just over 7 dB, while the example in Fig. 2 yields a result near 0 dB, and Fig. 3 just over 1.2 dB.

A weakness of these conditional requirements for identifying homogeneity is that cases where a cloud is directly above the radar but with gaps (or equally thin cloud) on both sides may be included. In effect, if a cloud really is centered over the radar, then it can be misinterpreted as a case of enhanced backscattering. However, as will be described in the next section, we have manually examined more than 250 of the RHI

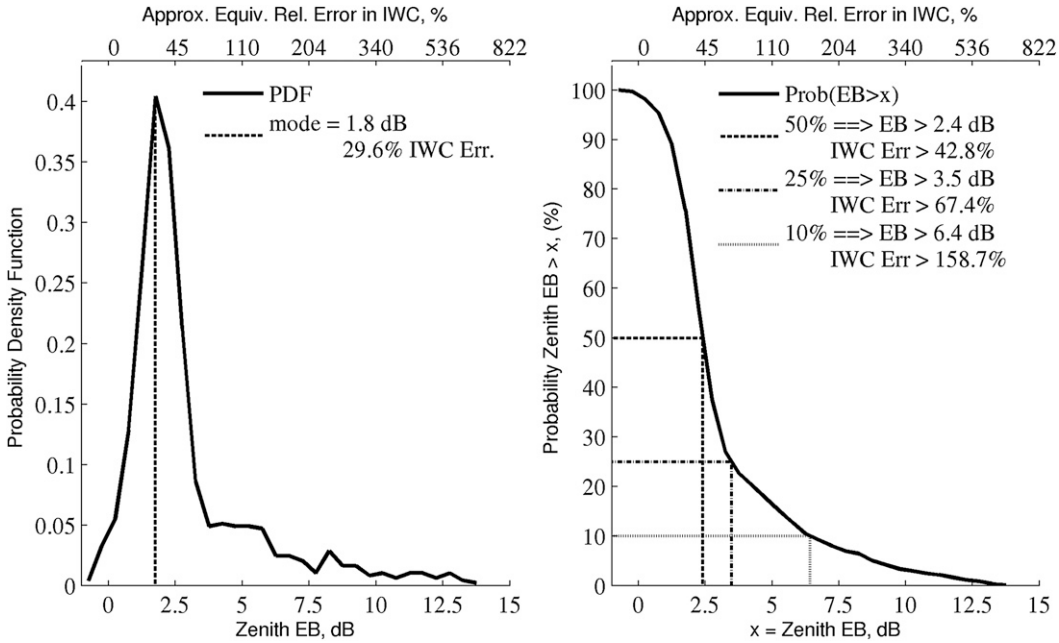

FIG. 4. (left) Probability distribution of zenith EB. (right) Cumulative distribution showing probability of zenith EB exceeding the value given on the horizontal axis. In both panels, the equivalent relative error in IWC is shown assuming power-law relationship IWC = aZ^b, where $b = 0.643$. The value of a does not affect the relative error [see text and Eq. (5)].

scans used in this analysis and found only 16 cases where this occurred or, more broadly, where we suspected that heterogeneity in the cloud had resulted in a bad retrieval. Removing these 16 cases had only a trivial effect on the statistics presented in the next section, giving us confidence that the homogeneity criteria are sufficient to capture the effect of oriented snow crystals on backscattering at W band.

Another limitation of the retrieval for Z_{EB} is that since only a narrow range of low-elevation angles can be used in estimating Z_{cloud} and Atten, the estimate of these parameters can be sensitive to small spatial-scale variability in the observed reflectivity. We will discuss this further in the context of the observations shown in the next section. Overall, we found that using a vertical interval from 0.5 to 1 km reduced the variability in the reflectivity versus elevation angle curve over using either a half-as-narrow or twice-as-wide vertical interval. Also, instead of applying the technique to each individual RHI scan, we averaged the six RHI scans collected over a total time span of about five minutes and fit the model [Eq. (2)] over a 10° range (rather than simply using the observed values at the end points). Both of these changes modestly improved the results by increasing the fraction of RHI scans that meet the requirements for homogeneity.

3. Analysis

During StormVEx, a total of 38 616 RHI scans were made, from which we obtained 6463 temporally averaged or composite RHI scans (each separated by about one-half hour). To ensure good signal-to-noise ratio in the associated depolarization ratio, we limited the analysis to those cases where the observed reflectivity at zenith was greater than −10 dBZe, which occurred in approximately 36% of these scans. The technique described in the previous section was applied to estimate the enhanced backscattering at zenith and path attenuation. This approach requires cloud that is horizontally homogenous over the region analyzed. The homogeneity conditions, described in the previous section, further reduced the analysis set to 983 RHI scans or about 15.3% of the possible 6463 RHI scans. This is more than 40% of the RHI scans with a zenith reflectivity greater than −10 dBZe.

Figure 4 shows the resulting probability distribution and cumulative distribution of the zenith EB. The data show that at least a small amount of zenith EB was present in most RHI scans, with the most probable value being 1.8 dB and a median value of 2.4 dB. While these values do not seem large, they will cause a nontrivial bias in radar-based retrievals of ice water content (IWC). While the exact error in IWC will, of course, depend on

the details of the IWC retrieval, we can gauge the error by noting that the relationship between IWC and radar reflectivity is often represented by a power-law relationship of the form $\mathrm{IWC}(Z) = aZ^b$, where a and b are constants (Sassen et al. 2002). Defining the relative error in IWC as

$$\mathrm{IWC\_rel\_err} = 100\left[\frac{\mathrm{IWC}(Z_{\mathrm{cloud}}) - \mathrm{IWC}(Z_{\mathrm{const}})}{\mathrm{IWC}(Z_{\mathrm{const}})}\right], \quad (4)$$

noting that $\mathrm{dB}(Z_{\mathrm{cloud}}) = \mathrm{dB}(Z_{\mathrm{const}}) + \mathrm{dB}(Z_{\mathrm{EB}})$ and substituting the above power-law expression into this definition, one obtains

$$\mathrm{IWC\_rel\_err} = 100[10^{0.1b\mathrm{dB}(Z_{\mathrm{EB}})} - 1]. \quad (5)$$

Thus a power-law relationship with a constant value of b results in a one-to-one relationship between the additional reflectivity because of enhanced backscattering and the relative error in IWC. This simple relationship is a consequence of the fact that we have defined Z_{EB} as a simple additive factor in logarithm space. A variety of values have been proposed for b, ranging from 0.58 to about 0.8 (Sassen et al. 2002). A reasonable value of $b = 0.643$ implies a median error of 2.4 dB is equivalent to a relative error or relative bias in IWC of about 43%. Larger values of b imply slightly larger errors. For example, using a value of $b = 0.8$ would yield a relative error of about 56%. While the median value of zenith EB is modest, the distribution is skewed toward larger values, with values exceeding 10 dB on a few occasions. Of the homogenous cloud cases, 25% had a zenith EB exceeding 3.5 dB (equivalent to a relative error in IWC near 67%) and 10% of the cases had a zenith EB exceeding 6.4 dB (equivalent to a relative error in IWC in excess of 150%).

The scatterplot in Fig. 5 examines the relationship between the zenith EB, the radar depolarization ratio, and the cloud particle types as determined from CPI observations at SPL. In this figure, the color symbols represent a variety of cloud particle categories as summarized in Table 1. Red symbols denote cases where planar ice crystals were observed, while circles of all colors represent cases where water droplets were the dominant (most numerous) cloud particle. The large numbers of red symbols and circles indicate that planar ice crystals and mixed-phased clouds were common.

This particle type classification was obtained by manual examination of particle images gathered by the CPI within 15 minutes of the associated RHI scan. All RHI scans where CPI data were available and that had a zenith EB greater than 4 dB or a DR Diff 45 (described below) greater than 4 dB were examined. In this region of the scatterplot, all gray diagonal crosses indicate times where CPI images were unavailable or captured only a few particles, insufficient to assign a particle category. Most often this occurred simply because the cloud base was just above SPL. However, periods with low particle concentrations may not be well represented and, while the CPI was aspirated, low winds speeds may reduce the size of the sampling volume, such that, our classification results may be biased to periods with stronger winds or larger particle concentrations. Particle fall speeds are also potentially a factor, as more slowly falling particles are less likely to pass through the sampling volume during the observation time window than larger particles. A randomly selected sample of points with values less than 4 dB was also examined. This sampling represents roughly half the points where CPI data were gathered. In total there are 122 points with a CPI-based particle-type classification.

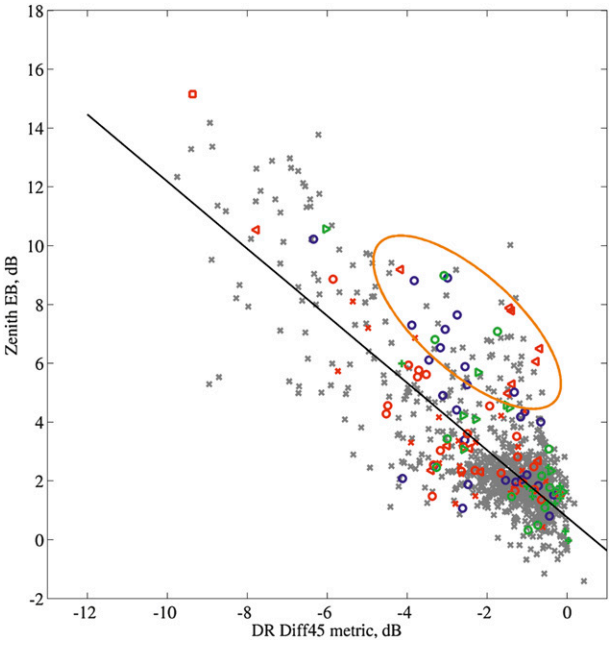

FIG. 5. Scatterplot showing relationship between zenith EB and change in DR given by Diff 45. Color symbols are defined in Table 1. Region identified by the orange ellipse is discussed in the text.

In Fig. 5, the difference in the observed depolarization ratio at zenith minus that observed at an elevation angle of 45°, which we call DR Diff 45, is shown along the horizontal axis. For planar particles, the depolarization ratio is expected to increase from values at zenith that are close to the radar polarization cross-coupling isolation limit (about −21.8 dB) for the ARM radar during StormVEx to a maximum value at the lowest elevation angles (Matrosov et al. 2012; see also middle-right

TABLE 1. Description of cloud particle classes and symbols used in figures. While particle columns were not rare, only on very few occasions were columns observed to be dominant habit. Field observations suggest there were periods with needles, aggregates composed of columns, aggregates composed of dendrites, aggregates composed of plates, and in one case, a polycrystal consisting of rounded heavily rimed particles with needlelike projections.

Symbol	Description
Red diagonal cross	Cloud dominated by pristine plates, sector plates, or dendrites. Few, if any, water drops and at most light riming. Some cases include columns or capped columns.
Red triangle	Cloud dominated by irregularly shaped planar structures. Typically heavily sublimated or partially melted dendrites. Original crystal structure is often uncertain. Little, if any, riming is present (but may have existed before melting), and water droplets are rare.
Red square	Zenith EB greater than 10 dB. CPI showed only a small number of ice crystals; all were large plates or large and broad columns. Some crystals were slightly rimed.
Red circle	Cloud dominated by water droplets, but at least one planar crystal was observed.
Blue circle	Cloud dominated by liquid water droplets to the point where identification of ice type is problematic. Fewer than five ice crystals observed, typically small and heavily rimed particles. No planar crystals are observed.
Green circle	Cloud dominated by water droplets, but heavily rimed particles or rimed columns are also present.
Green plus	Cloud dominated by heavily rimed particles. Water drops may be presented but not in large numbers. Original crystal habit is often difficult or impossible to determine or appears to be columns. In some cases, rimed or pristine columns are also present.
Green triangle	Cloud dominated by heavily rimed particles, some of which are very likely dendrites or plates. Water drops may be present, but not in large numbers. In some cases, rimed or small pristine columns are also present.
Gray diagonal cross	No classification possible or attempted.

panels of Figs. 1 and 3). Spherical particles, rounded (heavily rimed) irregulars, and columns are expected to produce little or no change in depolarization ratio with the elevation angle (Fig. 2). The choice of 45° used here for the elevation angle is guided by theoretical considerations for Ka band that suggest the impact of particle flutter on the slant linear depolarization ratio will be minimal around 45° (Reinking et al. 2002). However, we find no significant sensitivity in our results for any reasonable choice.

There are red symbols in Fig. 5 that have low zenith EB, demonstrating that the presence of planar crystals does not guarantee that zenith EB will be large. In most of these cases, in particular the mixed-phase clouds (red circles), planar crystals are not the dominant particle type. There are, however, a few cases where planar crystals are the most common particle type (red diagonal crosses). The CPI data for these cases show large numbers of small plates.

As expected, most of the cases where the CPI showed the ice particles to be heavily rimed (green symbols in Fig. 5) have only modest values for zenith EB and DR Diff 45. There are, however, a few cases where only heavily rimed particles were imaged by the CPI and yet there is a zenith EB or DR Diff 45 greater than 4 dB. Most of these cases appear to contain rimed dendrites or rimed plates (green triangles), and it is likely that some of these particles may continue to be horizontally oriented. It is also possible that relatively pristine planar crystals were present in these cases and simply not sampled by the CPI. Manual surface observations taken during StormVEx support this possibility. During the experiment a black felt surface was occasionally used to manually capture falling crystals for visual inspection of the crystal type, and on several occasions the collected samples revealed a multitude of heavily rimed particles with one or two seemingly miraculous pristine (or nearly pristine) sector plates or dendrites. CPI sampling limitations are certainly a factor with respect to the blue circles with large zenith EB. The blue circles represent cases where the CPI is dominated by water drops and imaged few, if any, ice particles. When cloud water is present, the number of water drops can greatly exceed the number of ice crystals, often by a factor of 100 or more. In these circumstances the CPI tends to spend most of its time imaging water drops, with little chance of capturing more rarely occurring ice particles (Lawson et al. 2006). However, measurements from particle sizing probes at SPL (specifically a Droplet Measurement Technology Particle Imaging Probe and Cloud Imaging Probe), which have larger sampling volumes, show that large ice particles were present in these cases. The CPI data are perhaps best used in confirming the presence of particle types and identifying the type of the most numerous or dominant particles, rather than trying to exclude or limit the range of particle types present. In the context of the present analysis, the CPI data certainly show that planar ice crystals were common, and that when these particles are present, there is strong correlation between DR Diff 45 and the estimated value for the zenith EB.

Including all points in Fig. 5, the correlation between DR Diff 45 and the zenith EB is about −0.79, indicating that about half the variation in zenith EB is captured by DR Diff 45. A least squares linear fit to the data is shown by the black line. The data are scattered about this line with a root-mean-square (RMS) difference of about 1.5 dB. The correlation coefficient and RMS fit indicate that measurements of the slant depolarization ratio could be used to improve radar-based retrievals [meaning that measurements of DR Diff 45 could be used to detect the presence of (some) oriented ice and perhaps estimate the size of the expected zenith enhancement in copolar reflectivity when needed, albeit with an RMS uncertainty of about 1.5 dB]. We note that DR Diff 45 requires radar measurements at only nadir and 45°, is not affected by path attenuation, and does not require the strict homogeneity conditions being used in the present analysis (though one would still be assuming the same particle shapes and orientations at both angles).

Perhaps surprisingly, Fig. 5 suggests that the largest zenith EB for any given value of DR Diff 45 (see the region highlighted by the orange ellipse in Fig. 5) often occurs when the cloud is primarily composed of irregularly shaped planar crystals (red triangles) that appear to be sublimating or melting planar crystals. The retrieval for the zenith EB given in section 2 assumes that the copolar reflectivity enhancement at low elevation angles is small compared to enhancement in the zenith direction (such that the cloud particle scattering is constant). We speculate that these larger EB values are at least partly because of the reflectivity being significantly impacted by the crystal orientation even at low elevation angles, perhaps because of there being few nonoriented ice crystals. Many of the largest enhanced backscattering cases appear to have occurred when small numbers of planar crystals were falling out of a mixed-phase region. The largest observed EB (the red square in Fig. 5) is one such case. The CPI data collected at this time show only a small number of ice crystals, all of which were large plates or large and broad columns (the only time such columns were observed in our sampling).

The linear fit in Fig. 5 has a nonzero intercept value of about 0.77 dB. This nonzero value could be due to a variety of causes. For example, the ARM radar had a rather poor cross-polar isolation of about −21.8 dB and it is possible that there are cases where the cross-polar reflectivity of oriented ice crystals is present but below the isolation level, and so is undetected. Another possibility is that the estimated attenuation could be biased high, which would cause the retrieved zenith EB to be biased high. However, examination of the attenuation retrieval results, which are discussed later in this section, suggests that the bias is smaller than 0.77 dB. Perhaps the most likely reason for the nonzero intercept is that nonspherical, irregular particles and columns, which are expected to generate little to no DR Diff 45 signal, cause a slight increase in zenith EB. An analysis of irregular (heavily rimed) particles observed from aircraft optical array probes by Hogan et al. (2012) indicates that most heavily rimed particles are not spherical, but are better modeled as oblate spheroids with an axial ratio near 0.6 (and typically ranging from case to case between about 0.5 and 0.75, and with some dependence on particle size). These authors found that using a horizontally oriented oblate spheroid model significantly improved the forward calculation of radar reflectivity (from the aircraft observation size distribution) compared against coincident observations from ground-based 9.7-GHz radar. The presence of relatively modest positive zenith EB values for CPI cases containing only heavily rimed particles (green pluses in Fig. 5), as well as the positive mode in the distribution of zenith EB in Fig. 4 with few data points near 0 dB, is consistent with irregular particles being nonspherical and having some horizontal orientation.

Both panels in Fig. 6 show scatterplots of the retrieved total path attenuation against DR Diff 45, the difference being that the left panel includes only cases where the total column liquid water path (LWP) estimated from measurements of the ARM microwave radiometer is less than 20 g m^{-2} and the right panel includes only cases where the LWP is greater than 20 g m^{-2}. Details on the ARM two-channel microwave radiometer retrieval are given by Liljegren (1999) and Westwater et al. (2001). The total path attenuation is due to both gasses (primarily water vapor) and cloud condensate (primarily liquid water). The purpose of the left panel is to provide insight into the retrieved attenuation when the contribution from liquid water must be small and the path attenuation is primarily due to water vapor. The right panel includes cases where there is significant attenuation due to liquid water, but also includes cases where the liquid water occurs above 1 km and so does not contribute to the path attenuation of the analyzed region of the cloud.

Because of the statistical technique used in the LWP retrieval, the retrieval is prone to produce both small negative and positive values for the LWP when there is no liquid water in the cloud, and in the case of supercooled liquid water there are relatively larger uncertainties because of uncertainties in the dielectric constant of liquid water below 0°C, which may bias the LWP retrieval (Westwater et al. 2001; Marchand et al. 2003). We have selected a conservative value for the LWP threshold of 20 g m^{-2}, which should ensure that the actual LWP is less than 50 g m^{-2}, equivalent to a

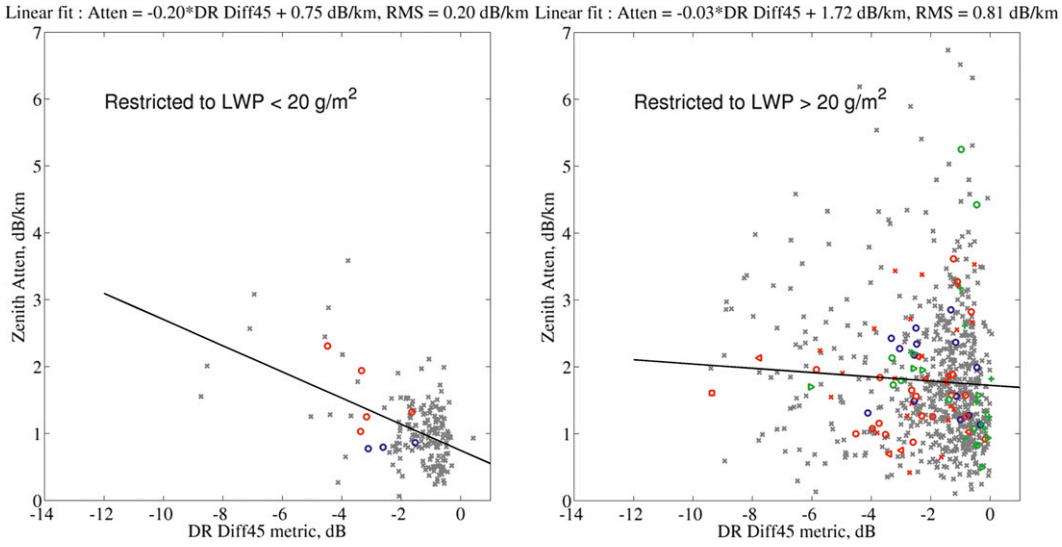

FIG. 6. Scatterplots showing relationship between retrieved path attenuation (vertical axis) and change in DR. Color symbols as in Fig. 5 and defined in Table 1. (left) Points where the total column LWP is estimated to be less than 20 g m^{-2}. (right) Points where the LWP is estimated to be larger than 20 g m^{-2}.

path attenuation of less than 0.2 dB km^{-1} at 94 GHz. For the range of pressures and temperatures present at StormVEx, the gaseous attenuation is expected to vary between about 0.3 and 0.8 dB km^{-1}. Thus, while some of the spread shown in the left panel of Fig. 6 is likely because of real variability in water vapor and small amounts of liquid water, much of the variability is because of error in the estimated value of attenuation. There are few cases where the estimated attenuation exceeds 2 dB km^{-1}. An examination of these cases shows that while some of these outliers may be because of heterogeneities in the observed cloud copolar reflectivity (i.e., small-spatial-scale variability in the reflectivity versus elevation angle curve), most cases show little heterogeneity; and we suspect these unreasonably large values for the path attenuation, are a result of violating the assumption that the cloud reflectivity is constant at low elevation angles—though it is also possible there has been a significant underestimate of the microwave-radiometer-retrieved LWP. Nonetheless, even with these outliers, the RMS variability is only about 0.2 dB km^{-1}, the mean value is near 1 dB km^{-1}, and the intercept value is near 0.7 dB km^{-1}, indicating there is little bias in the estimated path attenuation, perhaps a few tenths of a decibel per kilometer at most.

The right panel of Fig. 6 shows that liquid water adds significant path attenuation with a mean attenuation about 1 dB km^{-1} larger than the low-LWP cases shown in the left panel. An examination of the handful of cases where the estimated path attenuation is greater than 4 dB km^{-1} suggests these are not errors because of heterogeneity in the observed clouds but rather cases with large amounts of liquid water, including several cases where freezing drizzle may be present. We note that any attenuation due to liquid water (or wet snow) on the radar dome will also add to the path attenuation. With typical total path attenuation less than about 2 dB km^{-1}, cases where the enhanced backscattering exceeds 2 dB are usually visually easy to identify in the observed RHI scan and represent more than half of all cases.

4. Summary and discussion

In summary, an analysis of 95-GHz scanning radar data collected during StormVEx shows that at least a small amount of enhanced backscattering (EB) because of horizontally oriented ice crystals was present in most radar scans, with a median enhancement of 2.4 dB at zenith compared with reflectivity at low elevation angles. This is roughly equivalent to a relative bias error in ice water content (IWC) of about 43%. While the median value of the zenith EB is modest, the distribution is skewed toward larger values, with values occasionally exceeding 10 dB. In 25% of the cases, the zenith EB exceeded 3.5 dB (equivalent to a relative error in IWC in excess of 67%) and 10% of the cases had a zenith EB exceeding 6.4 dB (equivalent to a relative error in IWC in excess of 150%). These results suggest that without some means of identifying the effect of orientation on zenith or nadir backscatter, (bias) errors in the climatologies of radar-retrieved IWC for warm ice clouds

($T > -20$°C) or mixed-phase clouds should be anticipated, and are likely to be significant. The analysis also shows there is a strong correlation (about −0.79) between the change in slant 45° depolarization ratio with radar scan elevation angle and the magnitude of the zenith EB, suggesting that measurements of the slant depolarization ratio could be used to improve radar-based retrievals by helping account for ice crystal orientation.

Cloud particle imager data indicate that large enhancement typically occurred when planar crystals were present. While more modest enhancements were sometimes clearly a result of planar crystals, at other times the enhancement appears to be because of nonspherical irregularly shaped particles, consistent with the analysis of Hogan et al. (2012). These irregularly shaped particles often appear to be heavily rimed columns and broken dendrites, though this observation is somewhat speculative, as the rime makes the identification ambiguous. The largest enhancement seems to have occurred when large planar crystals were falling out of a liquid-water layer into a region with little ice condensate—conditions in which oriented and planar ice crystals have been noted to occur during other experiments (e.g., Westbrook et al. 2010; Carey et al. 2008; Hogan et al. 2003).

The retrieval for the zenith-enhanced backscattering used here is based on a simple model that assumes the radar backscattering at low elevation angles is only due to path attenuation and a constant cloud reflectivity. We do not expect the estimated value for enhanced backscattering obtained here to be the same as what one would get for scattering from the same particles being randomly oriented or relative to what one would get from spheres of the same mass. Our enhanced backscattering estimate represents a practical measure on the effect of oriented ice crystals and its strength will depend on many factors, including the relative abundance and size of oriented to nonoriented particles. The assumption of constant cloud reflectivity at low elevation angles may be violated when only oriented ice is present. In general, we expect changes in reflectivity because of oriented ice at low elevation angles to increase the estimate for the zenith EB, and this will depend slightly on the polarization state [as we expect the off-zenith copolar reflectivity measured with slant 45° depolarization will be smaller than that measured with horizontal-transmit horizontal-receive (HH) polarization, for example]. Regardless, cases where the change in scattering at low elevation angles is due to oriented ice crystals are certain to produce large errors in any radar-based retrieval for the ice water content that does not take the particle orientation into account. In general, a more sophisticated approach could be developed that uses a model for the oriented ice particle scattering with elevation angle. Such a retrieval would require deriving additional parameters, or making assumptions, constraining the shape of the size distribution, the axial ratio of the oriented ice crystal (with size), and the relative contribution of oriented particles to randomly oriented particles.

The results presented in section 3 are not sensitive to small changes in the thresholds used to ensure homogeneous conditions. For example, tightening the difference threshold between the estimated zenith EB from the two elevation angle ranges used from 1.5 to 1.0 dB changes the correlation coefficient from −0.79 to −0.8. While it is possible that enhanced backscattering differs under the conditions studied than in less homogenous conditions, we note that the analysis region is only 4 km wide and that the 983 composite scans included represent more than 40% of the total number of such scans where the zenith reflectivity was greater than −10 dBZe. The ridgeline upon which SPL sits runs north–south and the larger-scale midtropospheric flow usually had a strong westerly component. Local-scale flows at low levels were complicated, but cases where there was a strong low-level upslope flow were not rare. While topographic uplift at the radar site may be responsible for some amount of the inhomogeneity in the radar analysis region, a visual examination of the radar data suggests this was not a dominant factor. In regard to both Figs. 2 and 3, for example, the larger reflectivities are actually on the left side of the figure (that is, farther from the mountain), whereas one might expect any upslope flow to create larger water contents and particle sizes closer to the mountain. Also, comparison of reflectivity distributions at the edges of the analysis region (not shown) indicates no statistical difference when looking toward the ridgeline ($x = +2$ km) or away from the ridgeline ($x = -2$ km). The small size of the analysis regions is certainly key, as differences in the reflectivity distribution become evident when looking farther from the ridge (e.g., $x = +5$ km). The short distance between the radar and SPL also likely helps ensure that particle properties measured at SPL (2.4 km from the radar) are representative much of the time.

The radar data gathered during StormVEx are not well suited to studying the duration of oriented ice crystal events. The radar RHI scans (which took a total of about 5 min) were done only about once each half hour. So, even if we detect oriented ice crystals one-half hour apart in consecutive radar scans, we have no good way to know if they were present during the entire period between the scans. Also, the analysis technique was focused on homogeneous conditions and cases where

the radar scans at every half hour pass the homogeneity criteria for some extended period are infrequent. These issues aside, our visual interpretation is that there is no ''characteristic scale'' of oriented ice crystal occurrence, and there were events where oriented ice crystals were present for many consecutive hours and events where they occurred only briefly (for less than an hour, perhaps even only a few minutes).

Naturally, the question arises as to how representative StormVEx results might be of clouds in other regions. It seems possible or even likely that the orographic uplift created by the Park Range of the Rocky Mountains near Steamboat Springs is a key component in ensuring the temperatures and supersaturations needed for frequent and vigorous growth of planar crystals during StormVEx. Planar ice crystals have been frequently observed in other mountainous regions during the winter, for example, in wintertime systems passing over the Cascades during the Improvement of Microphysical Parameterization through Observational Verification Experiment (IMPROVE) field experiments in Oregon (Woods et al. 2005), as well as in many earlier surface and aircraft measurements in the Pacific Northwest Cascades (e.g., Hobbs 1975), and other mountains regions (e.g., Choularton et al. 2008; Sassen 1984; Rogers and Vali 1987). Nonetheless, as discussed in the introduction, both satellite and aircraft data show that oriented ice crystals do occur in other regions. In particular, low-level mixed-phase clouds with ice falling from thin supercooled liquid water layers are a common occurrence in the Arctic (Shupe et al. 2006), and in situ measurements have shown that these clouds sometimes (and perhaps often) contain dendrites, plates, and other crystal types that are likely to be oriented (e.g., Earle et al. 2011; Korolev et al. 1999). Of particular interest is that Korolev et al. (1999) observed sublimating irregularly shaped particles that appear quite similar to what we observed during StormVEx, and which we found to often show large zenith-enhanced backscattering. If oriented crystals are less frequent outside of mountainous regions, then it nonetheless seems likely that oriented crystals will cause equally large errors in millimeter-wavelength radar-based retrievals when they do occur. The Atmospheric System Research program is currently placing scanning polarimetric 95- or 35-GHz radars at all of its fixed sites, as well as in its two mobile instrument suites. Radar observations from these systems, perhaps along with observations from other scanning radars (such as the Chilbolton site), could be used to more quantitatively address this question, both with respect to the presence of (copolar) reflectivity enhancement and its relationship to depolarization ratio.

In regard to the depolarization ratio, the main reason a slant linear configuration was used during StormVEx is because slant linear is expected to be less susceptible to small flutter in the horizontal orientation of particles than the more traditional horizontal–vertical linear depolarization ratio (LDR; Reinking et al. 2002). Thus, we expect that an EB–LDR relation will be much noisier than the EB to slant linear DR relation, and suggest that field programs consider making observations using slant 45° depolarization in addition to LDR.

It is also noteworthy that enhanced backscattering was frequently observed both below and within cloud mixed-phase regions, but less frequently near cloud top. The lack of enhanced backscattering at cloud top is likely due to ice particles being smaller and possibly more spherical, though it could also be that they are less likely to be horizontally oriented (perhaps partly due to increased turbulence). The vertical variability and presence of oriented particles in regions where lidar will not be able to penetrate, their potentially large impact on copolar reflectivity observations, the likely size-dependent nature of crystal orientation, and the added complexity (degrees of freedom) that oriented particles introduce into the retrieval process, all argue strongly for further research into retrieval techniques that include radar measurements of different depolarization types (e.g., Matrosov et al. 2005) and/or multiwavelength reflectivity ratios that could be indicative of particle types (e.g., Kneifel et al. 2011; Leinonen et al. 2012).

Acknowledgments. The StormVEx campaign was supported by the Office of Biological and Environmental Research of the U.S. Department Energy (DOE) as part of the Atmospheric System Research program, the National Science Foundation, and the NASA *CloudSat* project. The Desert Research Institute's SPL is an equal opportunity service provider and employer, and is a permitee of the Medicine Bow–Routt National Forests. We would especially like to thank and acknowledge the hard work of many people who made this research possible, including the many DOE ATSC and ASR staff (especially, Kevin Widener, Nitin Bharadwaj, Rich Coulter, and Brad Orr), Storm Peak Laboratory (SPL) local volunteers, the Steamboat Ski and Resort Corporation, the U.S. Forest Service, the Grand Junction National Weather Service office, Stratton Park Engineering Company (SPEC) Incorporated, and all of the graduate students (Betsy Berry, Stewart Evans, Ben Hillman, Will Mace, Clint Schmidt, Carolyn Stwertka, Adam Varble, and Christy Wall), who put considerable effort into collecting data.

REFERENCES

Atlas, D., M. Kerker, and W. Hitschfield, 1953: Scattering and attenuation by non-spherical atmospheric particles. *J. Atmos. Terr. Phys.,* **3,** 108–119, doi:10.1016/0021-9169(53)90093-2.

Aydin, K., and C. Tang, 1997: Relationships between IWC and polarimetric radar measurands at 94 and 220 GHz for hexagonal columns and plates. *J. Atmos. Oceanic Technol.,* **14,** 1055–1063.

——, and J. Singh, 2004: Cloud ice crystal classification using a 95-GHz polarimetric radar. *J. Atmos. Oceanic Technol.,* **21,** 1679–1688.

Borys, R. D., and M. A. Wetzel, 1997: Storm Peak Laboratory: A research, teaching and service facility for the atmospheric sciences. *Bull. Amer. Meteor. Soc.,* **78,** 2115–2212.

Carey, L. D., J. Niu, P. Yang, J. A. Kankiewicz, V. E. Larson, and T. H. Vonder Haar, 2008: The vertical profile of liquid and ice water content in midlatitude mixed-phase altocumulus clouds. *J. Appl. Meteor. Climatol.,* **47,** 2487–2495.

Chepfer, H., G. Brogniez, P. Goloub, F. M. Breon, and P. Flamant, 1999: Observations of horizontally oriented ice crystals in cirrus clouds with POLDER-1/ADEOS-1. *J. Quant. Spectrosc. Radiat. Transfer,* **63,** 521–543, doi:10.1016/S0022-4073(99)00036-9.

Choularton, T. W., and Coauthors, 2008: The influence of small aerosol particles on the properties of water and ice clouds. *Faraday Discuss.,* **137,** 205–222, doi:10.1039/B702722M.

Clothiaux, E. E., T. P. Ackerman, G. G. Mace, K. P. Moran, R. T. Marchand, M. A. Miller, and B. E. Martner, 2000: Objective determination of cloud heights and radar reflectivities using a combination of active remote sensors at the ARM CART sites. *J. Appl. Meteor.,* **39,** 645–665.

Delanoë, J., and R. J. Hogan, 2010: Combined CloudSat–CALIPSO–MODIS retrievals of the properties of ice clouds. *J. Geophys. Res.,* **115,** D00H29, doi:10.1029/2009JD012346.

Earle, M. E., P. S. K. Liu, J. W. Strapp, A. Zelenyuk, D. Imre, G. M. McFarquhar, N. C. Shantz, and W. R. Leaitch, 2011: Factors influencing the microphysics and radiative properties of liquid-dominated Arctic clouds: Insight from observations of aerosol and clouds during ISDAC. *J. Geophys. Res.,* **116,** D00T09, doi:10.1029/2011JD015887.

Hallar, A. G., G. Chirokova, I. B. McCubbin, T. H. Painter, C. Wiedinmyer, and C. Dodson, 2011a: Atmospheric bioaerosols transported via dust storms in western United States. *Geophys. Res. Lett.,* **38,** L17801, doi:10.1029/2011GL048166.

——, D. H. Lowenthal, G. Chirokova, R. D. Borys, and C. Wiedinmyer, 2011b: Persistent daily new particle formation at a mountain-top location. *Atmos. Environ.,* **45,** 4111–4115, doi:10.1016/j.atmosenv.2011.04.044.

Heymsfield, A. J., 2003: Properties of tropical and midlatitude ice cloud particle ensembles. Part I: Median mass diameters and terminal velocities. *J. Atmos. Sci.,* **60,** 2573–2591.

Hobbs, P. V., 1975: The nature of winter clouds and precipitation in the Cascade Mountains and their modification by artificial seeding. Part I: Natural conditions. *J. Appl. Meteor.,* **14,** 783–804.

Hogan, R. J., P. N. Francis, H. Flentje, A. J. Illingworth, M. Quante, and J. Pelon, 2003: Characteristics of mixed-phase clouds. I: Lidar, radar and aircraft observations from CLARE'98. *Quart. J. Roy. Meteor. Soc.,* **129,** 2089–2116.

——, L. Tian, P. R. A. Brown, C. D. Westbrook, A. J. Heymsfield, and J. D. Eastment, 2012: Radar scattering from ice aggregates using the horizontally aligned oblate spheroid approximation. *J. Appl. Meteor. Climatol.,* **51,** 655–671.

Kneifel, S., M. S. Kulie, and R. Bennartz, 2011: A triple-frequency approach to retrieve microphysical snowfall parameters. *J. Geophys. Res.,* **116,** D11203, doi:10.1029/2010JD015430.

Korolev, A. V., G. A. Isaac, and J. Hallett, 1999: Ice particle habits in Arctic clouds. *Geophys. Res. Lett.,* **26,** 1299–1302, doi:10.1029/1999GL900232.

——, ——, and ——, 2000: Ice particle habits in stratiform clouds. *Quart. J. Roy. Meteor. Soc.,* **126,** 2873–2902, doi:10.1002/qj.49712656913.

Lawson, R. P., B. A. Baker, C. G. Schmitt, and T. L. Jensen, 2001: An overview of microphysical properties of Arctic clouds observed in May and July 1998 during FIRE ACE. *J. Geophys. Res.,* **106** (D14), 14 989–15 014.

——, D. O'Connor, P. Zmarzly, K. Weaver, B. Baker, Q. Mo, and H. Jonsson, 2006: The 2D-S (stereo) probe: Design and preliminary tests of a new airborne, high-speed, high-resolution particle imaging probe. *J. Atmos. Oceanic Technol.,* **23,** 1462–1477.

Leinonen, J., S. Kneifel, D. Moisseev, J. Tyynelä, S. Tanelli, and T. P. Nousiainen, 2012: Evidence of nonspheroidal behavior in millimeter-wavelength radar observations of snowfall. *J. Geophys. Res.,* **117,** D18205, doi:10.1029/2012JD017680.

Liljegren, J. C., 1999: Automatic self-calibration of ARM microwave radiometers. *Microwave Radiometry and Remote Sensing of the Earth's Surface and Atmosphere,* P. Pampaloni and S. Paloscia, Eds., CRC Press, 433–443.

Mace, J., and Coauthors, 2010: STORMVEX: The Storm Peak Lab Cloud Property Validation Experiment science and operations plan. U.S. Department of Energy Rep. DOE/SC-ARM-10-021, 44 pp.

Marchand, R., T. Ackerman, E. R. Westwater, S. A. Clough, K. Cady-Pereira, and J. C. Liljegren, 2003: An assessment of microwave absorption models and retrievals of cloud liquid water using clear-sky data. *J. Geophys. Res.,* **108,** 4773, doi:10.1029/2003JD003843.

Matrosov, S. Y., and A. J. Heymsfield, 2008: Estimating ice content and extinction in precipitating cloud systems from CloudSat radar measurements. *J. Geophys. Res.,* **113,** D00A05, doi:10.1029/2007JD009633.

——, R. F. Reinking, R. A. Kropfli, B. E. Martner, and B. W. Bartram, 2001: On the use of radar depolarization ratios for estimating shapes of ice hydrometeors in winter clouds. *J. Appl. Meteor.,* **40,** 479–490.

——, ——, and I. V. Djalalova, 2005: Inferring fall attitudes of pristine dendritic crystals from polarimetric radar data. *J. Atmos. Sci.,* **62,** 241–250.

——, G. G. Mace, R. Marchand, M. D. Shupe, A. G. Hallar, and I. B. McCubbin, 2012: Observations of ice crystal habits with a scanning polarimetric W-band radar at slant linear depolarization ratio mode. *J. Atmos. Oceanic Technol.,* **29,** 989–1008.

Noel, V., and H. Chepfer, 2004: Study of ice crystal orientation in cirrus clouds based on satellite polarized radiance measurements. *J. Atmos. Sci.,* **61,** 2073–2081.

——, and ——, 2010: A global view of horizontally oriented crystals in ice clouds from Cloud-Aerosol Lidar and Infrared Pathfinder Satellite Observation (CALIPSO). *J. Geophys. Res.,* **115,** D00H23, doi:10.1029/2009JD012365.

Okamoto, H., 2002: Information content of the 95-GHz cloud radar signals: Theoretical assessment of effects of nonsphericity and error evaluation of the discrete dipole approximation. *J. Geophys. Res.,* **107,** 4628, doi:10.1029/2001JD001386.

——, K. Sato, and Y. Hagihara, 2010: Global analysis of ice microphysics from CloudSat and CALIPSO: Incorporation of

specular reflection in lidar signals. *J. Geophys. Res.,* **115,** D22209, doi:10.1029/2009JD013383.

Reinking, R. F., S. Y. Matrosov, R. A. Kropfli, and B. W. Bartram, 2002: Evaluation of a 45° slant quasi-liner radar polarization state for distinguishing drizzle droplets, pristine ice crystals, and less regular ice particles. *J. Atmos. Oceanic Technol.,* **19,** 296–321.

Rogers, D. C., and G. Vali, 1987: Ice crystal production by mountain surfaces. *J. Climate Appl. Meteor.,* **26,** 1152–1168.

Sassen, K., 1984: Deep orographic cloud structure and composition derived from comprehensive remote sensing measurements. *J. Climate Appl. Meteor.,* **23,** 568–583.

——, and S. Benson, 2001: A midlatitude cirrus cloud climatology from the Facility for Atmospheric Remote Sensing. Part II: Microphysical properties derived from lidar depolarization. *J. Atmos. Sci.,* **58,** 2103–2112.

——, Z. Wang, V. I. Khvorostyanov, G. L. Stephens, and A. Bennedetti, 2002: Cirrus cloud ice water content radar algorithm evaluation using an explicit cloud microphysical model. *J. Appl. Meteor.,* **41,** 620–628.

——, V. K. Kayetha, and J. Zhu, 2012: Ice cloud depolarization for nadir and off-nadir CALIPSO measurements. *Geophys. Res. Lett.,* **39,** L20805, doi:10.1029/2012GL053116.

Shupe, M. D., S. Y. Matrosov, and T. Uttal, 2006: Arctic mixed-phase cloud properties derived from surface-based sensors at SHEBA. *J. Atmos. Sci.,* **63,** 697–711.

Stein, T. H. M., J. Delanoë, and R. J. Hogan, 2011: A comparison among four different retrieval methods for ice-cloud properties using data from *CloudSat*, *CALIPSO*, and MODIS. *J. Appl. Meteor. Climatol.,* **50,** 1952–1969.

Stephens, G. L., and Coauthors, 2008: CloudSat mission: Performance and early science after the first year of operation. *J. Geophys. Res.,* **113,** D00A18, doi:10.1029/2008JD009982.

Westbrook, C. D., A. J. Illingworth, E. J. O'Connor, and R. J. Hogan, 2010: Doppler lidar measurements of oriented planar ice crystals falling from supercooled and glaciated layer clouds. *Quart. J. Roy. Meteor. Soc.,* **136,** 260–276, doi:10.1002/qj.528.

Westwater, E. R., Y. Han, M. D. Shupe, and S. Y. Matrosov, 2001: Analysis of integrated cloud liquid and precipitable water vapor retrievals from microwave radiometers during the Surface Heat Budget of the Arctic Ocean project. *J. Geophys. Res.,* **106** (D23), 32 019–32 030.

Woods, C. P., M. T. Stoelinga, J. D. Locatelli, and P. V. Hobbs, 2005: Microphysical processes and synergistic interaction between frontal and orographic forcing of precipitation during the 13 December 2001 IMPROVE-2 event over the Oregon Cascades. *J. Atmos. Sci.,* **62,** 3493–3519.

Zhou, C., P. Yang, A. E. Dessler, Y. Hu, and B. A. Baum, 2012: Study of horizontally oriented ice crystals with CALIPSO observations and comparison with Monte Carlo radiative transfer simulations. *J. Appl. Meteor. Climatol.,* **51,** 1426–1439.